Debris Flows

C. Ancey

École Polytechnique Fédérale de Lausanne, Ecublens, 1015 Lausanne, Switzerland

1 Introduction

Debris flows are a major natural hazard, claiming thousands of lives and millions of dollars in lost property each year in almost all mountain areas on the Earth. After a catastrophic eruption of Mount St. Helens in the USA in May 1980, deposited ash and melting snow/ice produced very large debris flows and caused extensive damage and loss of life (Scott, 1988). During the 1985 eruption of Nevado del Ruiz in Colombia, more than 20,000 people perished when a large debris flow triggered by the rapid melting of snow and ice at the volcano summit swept through the town of Armero (Voight, 1990). In 1991, the eruption of Pinatubo volcano in the Philippines disperses more than 5 cubic kilometers of volcanic ash into surrounding valleys. Much of that sediment has subsequently been mobilized as debris flows by typhoon rains and has devastated more than 300 square kilometers of agricultural land. Even, in European countries, recent events that torrential floods may have very destructive effects (Sarno and Quindici in southern Italy in May 1998, where approximately 200 people were killed). In the summer of 1987, approximately 600 debris flows occurred after heavy rainfalls over many parts of Switzerland, causing substantial damage to inhabited areas (Rickenmann & Zimmermann, 1993).

The catastrophic character of these floods in mountainous watersheds is a consequence of significant transport of materials associated with water flows. Two limiting flow regimes can be distinguished. *Bed load* and*suspension* refer to dilute transport of sediments within water. This means that water is the main agent in the flow dynamics and that the particle concentration does not exceed a few percent. Such flows are typically two-phase flows. In contrast, *debris flows* are mass movements of concentrated slurries of water, fine solids, rocks and boulders. As a first approximation, debris flows can be treated as one-phase flows and their flow properties can be studied using classical rheological methods.

The study of debris flows is a very exciting albeit immature science, made up of disparate elements borrowed from geomorphology, geology, hydrology, soil mechanics, and fluid mechanics. The purpose of this chapter is to provide an introduction to physical aspects of debris flows, with specific attention directed to fluid-mechanics modeling. Despite attempts to provide a coherent view on the topic, coverage is incomplete and the reader is referred to a series of papers and books. A few books are particularly commendable (Brunsden & Prior, 1984; Coussot, 1997; Johnson & Rodine, 1984; Zimmermann *et al.*, 1997). Some review papers provide interesting overviews, introducing the newcomers to the field to the main concepts (Ancey, 2007; Chen, 1987; Coussot & Meunier, 1996; Iverson, 2005, 1997; Rickenmann, 1999; Takahashi, 1981).

2 Typology of torrential flows

2.1 Watershed as a complex physical system

The notion of torrent refers to a steep stream, typically in a mountainous context (Montgomery & Buffington, 1997; Wohl, 2000). According to a few authors, a stream can be referred to as a *torrent* as soon as its mean slope exceeds 6% (Bernard, 1927). For bed slopes ranging from 1% to 6%, it is called a *torrential river*. For bed slopes lower than 1%, it can be merely called a *river*. In addition to the slope, sediment supply is generally considered as another key ingredient in torrential watersheds. Depending on the nature of the soil and relief, slopes can provide a large quantity of poorly sorted solid materials to torrents. Supplied materials have sizes ranging typically from 1 µm to 10 m. The situation is very different from the one encountered for streams on an alluvial plain, where bed material is much finer and sorted (typically 1 µm to 10 cm) since it generally results from transport that occurred during previous floods (Church, 2006). Finally, one of the chief ingredients of torrential watersheds is water. Due to the small dimensions of torrential watersheds (typically from $0.1\,\mathrm{km}^2$ to $100\,\mathrm{km}^2$) and the steep slopes, floods are sudden, short, and violent. The flood regime differs significantly from plain floods, which are characterized by slower kinetics and smoother variations with time.

Figure 1 depicts a typical watershed. The upper part is generally degraded and submitted to erosion to a more or less large extent. It supplies water and sediment to the floods. Below this basin, the torrent enters a gorge, sometimes with very abrupt flanks depending on the nature of the soil. Then the torrent discharges onto the alluvial fan. The slope transition between the gorge and the alluvial provides interesting information on bed equilibrium. Generally, a watershed with an abundant supply of sediment and intense bed load transport in the past is characterized by a smooth transition from channel to fan.

Fig. 1: A typical watershed: the Brandy torrent (Savoie, France).

For plain rivers, sediment transport results from the action of water: water entrains materials either by pushing them along the bed (bed load transport) or by keeping them in suspension as a result of turbulence (suspension) (Garcia *et al.*, 2007). In a torrential context, as soon as the bed inclination is sufficiently high, gravity has a more pronounced role on sediment transport (Wohl, 2000; Armanini & Gregoretti, 2005). Therefore, on the one hand, bed load transport is more intense and on the other hand, a new mode of transport arises: debris flow. We can define them as follows:

- *Debris flows* are highly concentrated mixtures of sediments and water, flowing as a single-phase system. Debris flows look like mudslides and landslides except that their velocity and the distances they travel are much larger. It is worth noticing that in the literature there are many terms used to refer to slides and/or debris flows, which is a source of confusion.

- *Bed load transport* involves transportation of sediment by water. Coarse particles (sand, gravel, and boulders) roll and slide in a thin layer near the bed. Generally fine particles (silts and clays) are brought into suspension as a result of water turbulence. The system is typically made up of two distinct phases: the liquid phase (water) and dispersed (solid) phase.

2.2 Types of transport

In the laboratory, it is possible to simulate torrential phenomena using an inclined channel with a mobile bed made up of sand and gravel. Figures 2 and 3 show two very different situations that can be observed when the channel slope is increased by only a few percent. Figure 2(a) corresponds to a slope of 17%. At high discharges, fine particles are in suspension while the coarsest particles are pushed down to the bed. In this photograph, the largest particles are stationary and significantly affect water flow. The two phases (solid and liquid) are well separated and water flows much faster than solid particles. When the inclination exceeds a critical value (approximately 20%), a transition from a two-phase flow to a single-phase flow occurs very quickly. The mixture takes on the appearance of a homogeneous fluid flowing down the bed. Figure 2(b) (slope of 27%) illustrates such a transition and the resulting mass movement. Most laboratory experiments conducted with water flows on erodible beds have shown that the bed inclination θ is a key factor in sediment transport dynamics (Rickenmann, 1992; Smart & Jaeggi, 1983; Tognacca, 1999). On the whole it has been observed that:

- For $\theta < 20\%$: at sufficiently high water discharges, water flow induces intense bed load transport near the bed. As a first approximation, the water and solid discharges (respectively q_w and q_s) are linearly linked: $q_s \approx 8.2\,\theta^2 q_w$; note that this relationship is an overly simplified expression of discharge obtained by Smart & Jaeggi (1983) or Rickenmann (1992, 1997). Three layers can be distinguished: the bed made up of stationary particles (that can be eroded), the (active) bed layer in which sediment of all sizes is set in motion (rolling and sliding), and the water layer, where fine particles are in suspension or in saltation. In two-phase flows of this type the solid concentration (ratio of solid volume to total volume) does not exceed 30%.

- For $\theta > 20\%$: at sufficiently high water discharges, bed load transport is unstable. It changes into a dense single-phase flow. The solid concentration is very high, ranging from 50% to 90% depending on the particle-size distribution. Such flows simulated in the laboratory correspond to debris flows in the field.

(a)


(b)


Fig. 2: (a) Small-scale simulation of bed load transport in the laboratory. The solid and liquid phases are distinct (water was colored with fluoresceine). The typical flow depth in these experiments was 1 cm. (b) Small-scale simulation of a debris flow in the laboratory resulting from the "liquefaction" of the granular bed. The solid and liquid phases are well mixed. The photograph shows the snout propagating along the bed and eroding the upper layer.

In the laboratory, the transition from bed load transport to debris flow is reflected by a discontinuity in the solid concentration. It is suspected that such a discontinuity still exists in the field, at least in the Alps, but the underlying mechanisms are unknown. It is worth noticing that in the field, debris flows can also form from landslides (Iverson *et al.*, 1997). In this case, the transformation mechanisms are similar to soil liquefaction processes (rapid creep of saturated soils). In the following, we will focus on debris flows.

3 Initiation, motion, effects of debris Flow

3.1 Initiation

The torrential activity of a watershed depends on many parameters. Debris flows are common in some areas and uncommon in others. In areas prone to debris flow formation, their frequency also varies. In some watersheds, several debris flows occur each year while for other torrents, they are rare. Conditions for initiation of most debris flows usually include (Iverson, 1997; Iverson *et al.*, 1997; Coe *et al.*, 2008; Montgomery *et al.*, 2009):

- *Steep slopes.* In the Alps, slopes in excess of 70% are liable to surface erosion (sediment transport induced by runoff) and landslides (soil failure leading to large masses of saturated materials coming loose).
- *Abundant supply of unconsolidated materials.* Debris flows originate either from the simultaneous contributions of many material sources or from a single source (landslides):
  - Slow and continuous erosive processes on slopes in the drainage basin form deposits of materials in the torrent bed. Such deposits can be subsequently mobilized during intense floods and then transform into debris flows. In this case, debris flow originate as a slurry, primarily of water and fine particles, which erodes its channel and grows in size. Presumably instabilities in the bed load transport (such as those observed in the laboratory) arise and enable debris flow initiation. Usually the volume produced every year by erosion over the whole drainage basin is small and thus the amount of sediments that can be involved by a single debris flow is limited ($< 10^5\,\mathrm{m}^3$). In the field, the absence of failure surfaces and the presence of rills in the drainage basin are generally evidence that a debris flow has picked up coarse materials from the bed.
  - Old ill-consolidated deposits (moraines, massive rockfall deposit, etc.) can mobilize into landslides to form debris flows. In this case, the volume of materials involved can be very large ($> 10^5\,\mathrm{m}^3$) depending on the total volume made available by the source. Likewise, certain soils (e.g. gypsum) are very liable to landslides and can supply materials to debris flows. Presumably, initiation is due to a combination of several mechanisms: rapid creep deformation, increase in pore pressure, increase in load, erosion at the foot of the landsliding mass, etc. In the field, the presence of a failure surface can clearly serve to identify the source of material.
- *Large source of moisture.* Most of debris flows occur during or after heavy and/or sustained rainfalls. In some cases, snowmelt can be sufficient to form debris flows. There are many other ways in which water can be provided for the formation of debris flows: thawing soil, sudden drainage of lakes, dam break, etc., but these are much less frequent. A high liquid water content seems to be a necessary condition for the soil to be saturated, which causes: intense surface runoff, and an increase in the pore–water pressure (presumably leading to Coulomb slope failure).
- *Sparse vegetation.* Vegetation plays a role by intercepting rainfall (limitation of runoff) and increasing soil cohesion (root anchorage). Vegetation reduces the initiation potential to a certain extent but does not completely inhibit formation of debris flows. Many observations have shown that debris flows also occur in forested areas.

3.2 Motion

On the whole, debris flows are typically characterized by three regions, which can change with time (see Fig. 3):

- At the leading edge, a granular front or snout contains the largest concentration of big rocks. Boulders seem to be pushed and rolled by the body of the debris flow. The front is usually higher than the rest of the flow. In some cases no front is observed because either it has been overtaken by the body (this is very frequent when the debris flow spreads onto the alluvial fan), or the materials are well sorted and no significant variation in the bulk composition can be detected.
- Behind the front, the body has the appearance of a more fluid flow of a rock and mud mixture. Usually, the debris flow body is not in a steady state but presents unsteady surges. It can transport blocks of any size. Many authors have reported that boulders of relatively small size seem to float at the free surface while blocks of a few meters in size move merely by being overturned by the debris flow. The morphological characteristics of the debris flow are diverse depending on debris characteristics (size distribution, concentration, mineralogy) and channel geometry (slope, shape, sinuosity, width). Debris-flow velocity varies very widely but, on the whole, ranges from 1 m/s to 10 m/s (Major, 1996). The fastest debris flows are reported to move at more than 20 m/s (Major, 1996). Flowing debris can resemble wet concrete, dirty water, or granular material but whatever the debris characteristics and appearance, viscosity is much higher than for water. Most of the time, debris flows move in a completely laminar fashion, but they can also display minor turbulence; on some occasions, part of the debris flow may be highly turbulent.
- In the tail, the solid concentration decreases significantly and the flow looks like a turbulent muddy water flow.

In recent years, many outdoor and laboratory experiments have shed light on the connections existing between particle-size distribution, water content, and flow features for fixed volumes of bulk material (Davies, 1986; Iverson, 1997; Parsons *et al.*, 2001; Chambon *et al.*, 2009). In particular, experiments performed by Parsons *et al.* (2001) and Iverson (1997) have shown that the flow of poorly sorted materials was characterized by the coexistence of two zones, each one with a distinctive rheological behavior: the flow border was rich in coarse-grained materials (Coulomb frictional behavior), while the core was fine-grained (viscoplastic behavior). This self-organization has a great influence on the flow behavior; notably the run-out distance can be significantly enhanced as a result of levee formation limiting lateral spreading.

Parsons *et al.* (2001) ran a series of experiments to investigate the transition between viscoplasticity-dominated and friction-dominated regimes. They used a semi-circular inclined flume and measured the velocity profile at the free surface. Different slurries were prepared by altering the sand, clay, and silt fractions. They obtained muddy slurries, when the matrix was rich in silt and clay, and poorly sorted mixtures, when the silt and clay contents were reduced. Surprisingly enough, the change in the fine-particle content did not significantly modify the appearance of the body, whereas it markedly altered the composition

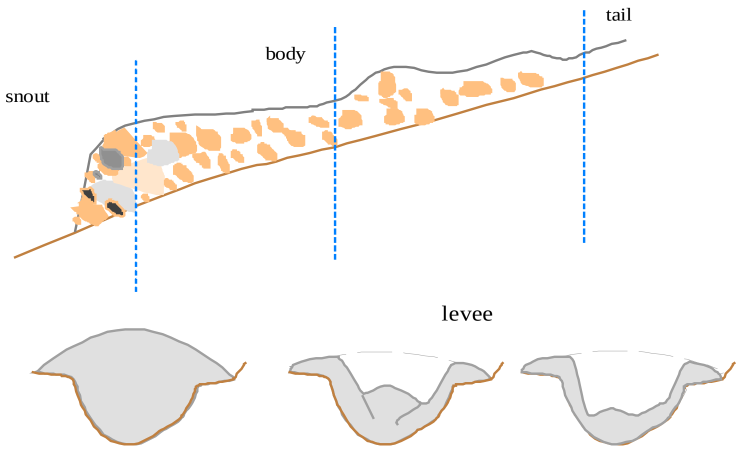

Fig. 3: Idealized representations of a debris flow (longitudinal profile and cross section). The different sections correspond to the dashed lines of the upper panel. Adapted from (Johnson & Rodine, 1984).

of the front and its behavior. Reducing the fine fraction in the slurries induced a radical change of behavior for the front (see Fig. 4):

- For muddy slurries, the front takes the form of a blunt nose. Lack of slip along the flume bottom caused a conveyer-belt-like flow at the front.
- For coarse-grained slurries, the front takes the form of a dry granular locked nose slipping along the bed as a result of the driving force exerted by the fluid accumulating behind the snout. Additional material was gradually incorporated into the snout, which grew in size until it was able to slow down the body.

Interestingly enough, the changes in the rheological properties mainly affected the structure of the flow, especially within the tip region.

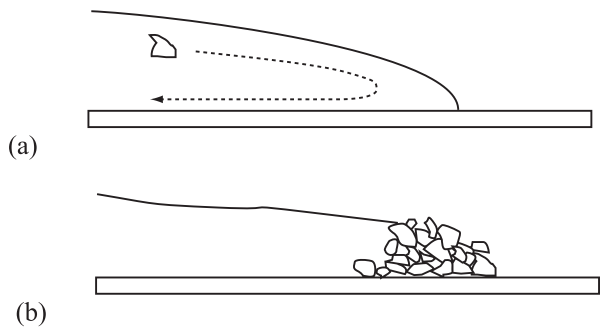

Fig. 4: Schematic of the behavior contrast between fine-grained and coarse-grained flows. (a) Conveyer-belt-like flow at the front. (b) Formation of a frictional front. After Parsons *et al.* (2001).

Iverson, Denlinger, and Major investigated slurries predominantly made up of a water-saturated mixture of sand and gravel, with a fine fraction of only a few percent (Major, 1996; Iverson, 1997, 2003*a*, 2005). Experiments were run by releasing a volume of slurry (approximately 10 m^3) down a 31-degree, 95-m-long flume. At the base of the flume, the material spread out on a planar, nearly horizontal, unconfined runout zone. Flow-depth, basal normal stress, and basal interstitial-flow pressure were measured at different places along the flume. Iverson and his co-workers observed that at early times, an abrupt front formed at the head of the flow, followed by a gradually tapering body, then a thin, more watery tail. The front remained relatively dry (with pore pressure dropping to zero) and of constant thickness, while the body elongated gradually in the course of the flow. Over the longest part of the flume, the basal pore pressure nearly matched the total normal stress, which means that shear strength was close to zero and the material was liquefied within the body (Iverson, 1997).

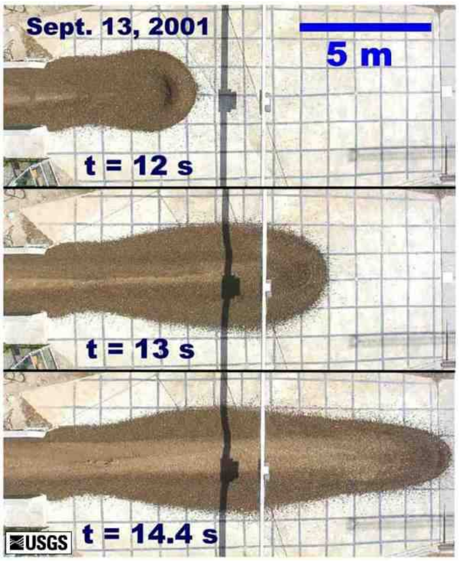

Fig. 5: Snapshots showing slurry flow discharging from the U.S. Geological Survey Debris-flow Flume and crossing the unconfined, nearly horizontal runout zone. The dark-toned material around the perimeter of the flow was predominantly gravel, while the light-toned material in the center of the flow was liquified mud. Figure reproduced from (Iverson, 2003*a*); courtesy of Richard M. Iverson.

Figure 5 shows a sequence of aerial photographs taken when the material spread out on the runout surface. Self-organization of the slurry flow into a coarse-grained boundary and a muddy core became quite visible as the flow traveled the runout surface. Lateral levees were formed by the granular front and confined the ensuing muddy body. Note the levee formation is probably not induced by particle segregation since it is also observed for dry granular flows involving spherical equal-size particles (Félix & Thomas, 2004). Figure 6 shows the lateral levees, which can be used to evaluate the cross-section of the flow,

Fig. 6: Cross-section of the Malleval stream after a debris flow in August 1999 (Hautes-Alpes, France).

while Fig. 7 shows a granular levee formed by a debris flow on the alluvial fan.

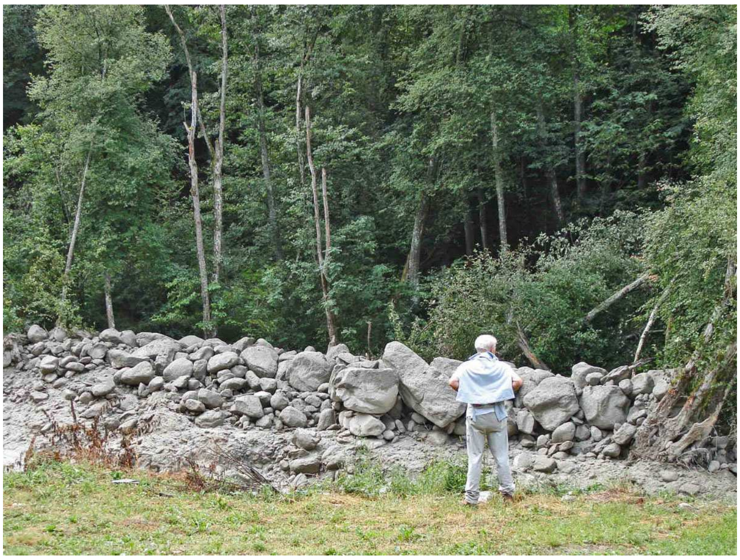

Fig. 7: Levees left by a debris flow in the Dunant river in July 2006 (Valais, Switzerland). Courtesy of Alain Delalune.

3.3 Deposition and effects

The distance that a debris flow can travel depends a great deal on the mechanical characteristics of the debris as well as the total volume, channel geometry and bed inclination. For instance it is generally observed that a debris flow moving over a flat tilted plane thins by spreading laterally and stops suddenly, seemingly when the thickness reaches a critical value. In contrast, if the debris flow is channelized, it may travel quite a long distance over gentle slopes. In European alpine countries, debris flows (of sufficient volume) generally begin to decelerate when the slope ranges from 10% to 25%. For some torrents, (e.g. Illgraben in Switerland and Boscodon in France), debris flows can propagate over gentle slopes (of less than 5%). In volcanic soil areas, it has been also demonstrated that lahars (debris flows involving water–ash mixtures) can propagate over very slight slopes (less than 1%) (Major, 1996).

For some debris flows, constant deposition occurs all along the channel and forms levees on the lateral boundaries of the torrent (see Figs. 6 and 7). Depending on the size distribution of the materials involved in the debris flow, a levee can have various shapes. In most cases, the cross section reveals a curved profile and, when the deposit is dry, it is characterized by strong cohesion. In other cases, the cross section has a straight free surface and even when it is dry, the deposit displays minor cohesion and looks like a sand or gravel heap. Formation of levees is not systematic. Many observers have noticed that, after a debris flow has passed through a channel, the channel bottom and sides have been swept clean of debris.

The alluvial fan is the preferential area for debris-flow deposition owing to the decrease in bed slope and widening of the channel. The slope decrease usually leads to the sudden stopping of the granular front and increase in the flow depth for the body. In many cases, debris flows overflow the channel banks and spread as broad lobes on the alluvial fan. As for levees, the morphological features of lobes vary widely. For instance, the longitudinal profile of a lobe margin can be curved (parabola-shaped), straight and tilted, or step-shaped. In the latter case, the deposit looks like an alluvial deposit. Although they move at low velocities on the alluvial fan, debris flows can impact or bury structures. Figure 8 shows the deposit of a large debris flow, which came down to inhabited areas.

4 Modeling debris flows

4.1 Debris flow classification and rheological behavior

The diversity in the morphological features of debris flows provides evidence of different families with specific bulk behavior. Several classifications have been proposed in the last few years. To date, there is no agreement on the chief characteristics on which classification should rely. Therefore, some classifications are based on the size distribution of materials involved, others only consider the mode of release, etc. Here we are mainly interested in the manner in which a debris flow propagates and therefore we suggest using a classification based on bulk mechanical behavior. We shall therefore consider three families (Bardou *et al.*, 2003):

Fig. 8: Debris flow deposit in Fully (Valais, Switzerland) in October 2000 (Courtesy of Crealp).

- *Muddy debris flow.* The transported material is usually characterized by a wide particle-size distribution. It is sufficiently rich in clay-like materials for the matrix to have a muddy consistency and lubricate contact between coarse particles. Most of the time, bulk behavior is typically viscoplastic. That means that the material exhibits both plastic and viscous properties (Major & Pierson, 1992; Phillips & Davies, 1991; Coussot, 1997; Bardou *et al.*, 2007; Sosio & Crosta, 2009). When the stress level is low, the material behaves as a solid body, but when the stress level exceeds of a critical value (yield stress), it flows as a fluid does. This yield stress confers specific properties to the material. For instance, when a given volume of material is released and spreads down a tilted flat plane, the flow depth decreases regularly. When the flow depth reaches a critical value (depending on the yield stress and the plane inclination), the driving shear stress is lower that the yield stress and the flow stops abruptly. In most cases, the yield stress ranges from 0.5 kPa to 15 kPa. Muddy debris flows can usually propagate over slopes greater than 5%. The limits of deposits are sharp and well delineated. Boulders and gravel are randomly distributed in a finer-grained cohesive matrix. Muddy debris flows are very frequent in the Alps.

- *Granular debris flow.* Although the size distribution is wide, the material is poor in fine (clay-like) particles. Bulk behavior is expected to be frictional-collisional (Takahashi, 1991; Ancey, 2001; Chen, 1987; Jenkins, 1994): it is mainly governed by collisions and friction between coarse particles. Energy dissipation is usually much larger for granular debris flows than for muddy debris flows and thus, granular debris flows require steep slopes ($> 15\%$) to flow. Presumably, as for very large rockfalls, a granular debris flow involving a very large amount of materials may travel large distances over more gentle slopes. In the field, deposits are easily recognized by the irregular chaotic surface. Deposits are generally graded, with coarser debris forming mass deposits and finer debris transported downstream (due to drainage).

- *Lahar-like debris flow.* The particle-size distribution is narrow and the material contains only a small proportion of clay-like materials. This type of debris flow is typical of volcanic soil areas (soils made up of fine ash), but it can be observed on other terrain (e.g. gypsum, loess) (Wan & Wang, 1994). Bulk behavior is expected to be frictional/viscous: at low shear velocities, particles are in sustained frictional contact and bulk behavior may be described using a Coulomb frictional equation. At high shear velocity, due to dilatancy and increased fluid inertia, contacts between coarse grains are lubricated by the interstitial fluid (Ancey & Coussot, 1999; Ancey, 2001). In the laboratory, such materials exhibit very surprising properties: at rest, they look like fine soil (silts) but once they have been stirred up, they liquefy suddenly and can flow nearly as Newtonian fluids. Contrary to muddy debris flows, the yield stress is low and therefore, lahars can move over gentle slopes of less than 1%. Deposits are very thin and flat, and look like alluvial deposits.

4.2 Rheometry

Natural suspensions are made up of a great diversity of grains and fluids. This observation motivates fundamental questions: how to distinguish between the solid and fluid phases? What is the effect of colloidal particles in a suspension composed of coarse and fine particles? We shall see that, when the particle size distribution is bimodal (i.e, we can distinguish between fine and coarse particles), the fine fraction and the interstitial fluid form a viscoplastic fluid embedding the coarse particles, as suggested by Sengun & Probstein (1989*a*); this leads to a wide range of viscoplastic constitutive equations, the most common being the Herschel-Bulkley model. The bimodal-suspension approximation usually breaks for poorly sorted slurries. In that case, following Iverson and his co-workers (Iverson, 1997, 2005), we will see that Coulomb plasticity can help understand the complex, time-dependent rheological behavior of slurries.

Over the last 20 years, a large number of experiments have been carried out to test the rheological properties of natural materials. The crux of the difficulty lies in the design of specific rheometers compatible with the relatively large size of particles involved in geophysical flows. Coaxial-cylinder (Couette) rheometers and inclined flumes are the most popular geometries. Another source of trouble stems from disturbing effects such as particle migration and segregation, flow heterogeneities, fracturation, layering, etc. These effects are often very pronounced with natural materials, which may explain the poor reproducibility of rheometrical investigations (Major & Pierson, 1992; Contreras & Davies, 2000; Iverson, 2003*b*). Poor reproducibility, complexity in the material response, and data scattering have at times been interpreted as the failure of the one-phase approximation for describing rheological properties (Iverson, 2003*b*). In fact, these experimental problems demonstrate above all that the bulk behavior of natural material is characterized by fluctuations that can be as wide as the mean values.

Authors	Experiments
O'Brien & Julien (1988)	viscometric tests on natural mudflow deposits
Coussot (1997), Coussot & Piau (1995), Coussot *et al.* (2003)	Couette rheometer on fine mud samples
Coussot *et al.* (1998)	wide-gap Couette rheometer with debris-flow samples
Bardou *et al.* (2003)	Couette rheometer and special rheometers used for concrete on debris-flow samples
Remaître *et al.* (2005)	Couette rheometer on fine mud samples
Major & Pierson (1992)	Couette rheometer with fine-grained materials collected on debris-flow deposits
Martino (2003)	Couette rheometer with natural samples
Schatzmann *et al.* (2003)	special BMS rheometer with natural samples
Parsons *et al.* (2001)	flume with artificial mixtures made up of clay, silt, and sand
Sosio & Crosta (2009)	Couette rheometer on sand and clay samples

Tab. 1: Experimental investigations conducted on natural materials or nearly natural materials providing evidence of viscoplastic behavior.

As for turbulence and Brownian motion, we should describe not only the mean behavior, but also the fluctuating behavior to properly characterize the rheological properties. For concentrated colloidal or granular materials (Lootens *et al.*, 2003; Tsai *et al.*, 2001), experiments on well-controlled materials have provided evidence that to some extent, these fluctuations originate from jamming in the particle network (creation of force vaults sustaining normal stress and resisting against shear stress, both of which suddenly relax). Other processes such as ordering, aging, and chemical alteration occur in natural slurries, which may explain their time-dependent properties (Marquez *et al.*, 2006). Finally, there are disturbing effects (e.g., slipping along the smooth surfaces of a rheometer), which may bias measurement. Table 4.2 reports a number of experimental investigations run on natural samples collected in the field or materials mimicking natural materials. The list is far from exhaustive. For Coulomb plastic materials, Major *et al.* (1997) and Major (1997, 2000) carried out geotechnical tests on natural samples while Denlinger & Iverson (2001), Iverson (1997), and Major (1996) investigated unsteady avalanches mobilizing natural mixtures down a long steep flume. Apart from these authors, most authors have tried to document that shear stress depends on the solid concentration or the shear rate, as expected from kinetic theory or Bagnold-like phenomenological laws (Takahashi, 1991; Aragon, 1995; Armanini *et al.*, 2005; Egashira *et al.*, 2001; Tubino & Lanzoni, 1993; Pouliquen & Forterre, 2002; Nishimura *et al.*, 1998). These authors are not cited in Table 4.2.

When the bulk is made up of fine colloidal particles, phenomenological laws are used to describe rheological behavior. One of the most popular is the Herschel-Bulkley model, which generalizes the Bingham law

$$\tau = \tau_c + K\dot{\gamma}^n, \tag{1}$$

with τ_c the yield stress, K and n two constitutive parameters. In practice, this phenomenological expression successfully describes the rheological behavior of many materials over a sufficiently wide range of shear rates (Bird *et al.*, 1983), except at very low shear rates (Coussot *et al.*, 2002). For numerical purposes, a viscoplastic model may be regularized using a biviscous model (Wilson *et al.*, 2002), Papanastasiou's exponential model Papanastasiou (1987), or extended forms Zhu *et al.* (2005). Indeed, the existence of a yield stress entails numerical difficulties in tracking the shape and position of the yield surface(s) within the flow.

When the bulk is made up of coarse noncolloidal particles, Coulomb friction at the particle level imparts its key properties to the bulk, which explains (i) the linear relationship between the shear stress τ and the effective normal stress $\sigma' = \sigma - p$ (with p the interstitial pore pressure)

$$\tau = \sigma' \tan\varphi, \tag{2}$$

and (ii) the non-dependence of the shear stress on the shear rate $\dot{\gamma}$. Some authors have suggested that in high-velocity flows, particles undergo collisions, which gives rise to a regime referred to as the frictional-collisional regime. The first proposition of bulk stress tensor seems to be attributable to Savage (1982), who split the shear stress into frictional and collisional contributions

$$\tau = \sigma \tan\varphi + \mu(T)\dot{\gamma}, \tag{3}$$

with T the granular temperature. Elaborating on this model, Ancey & Evesque (2000) suggested that there is a coupling between frictional and collisional processes. Using heuristic arguments on energy balance, they concluded that the collisional viscosity should depend on the Coulomb number $\mathrm{Co} = \rho_p a^2 \dot{\gamma}^2/\sigma$ (called the inertial number by Jop *et al.* (2005) and part of the French granular-flow community) to allow for this coupling in a simple way

$$\tau = \sigma \tan\varphi + \mu(\mathrm{Co})\dot{\gamma}. \tag{4}$$

Jop *et al.* (2005) proposed a slightly different version of this model, where both the bulk frictional and collisional contributions collapse into a single term, which is a function of the Coulomb number

$$\tau = \sigma\ \tan\varphi(\mathrm{Co}). \tag{5}$$

Contrasting with other propositions, (Josserand *et al.*, 2004) stated that the key variable in shear stress was the solid concentration ϕ rather than the Coulomb number

$$\tau = K(\phi)\sigma + \mu(\phi)\dot{\gamma}^2, \tag{6}$$

with K a friction coefficient. Every model is successful in predicting experimental observations for some flow conditions, but to date, none is able to describe the frictional-collisional regime for a wide range of flow conditions and material properties.

When the bulk is a bimodal suspension of coarse particles within a colloidal dispersion, it still behaves like a viscoplastic material. Sengun & Probstein (1989*a*,*b*) proposed different arguments to explain this behavior. Their explanation consists of two approximations. First, as this is the interstitial phase, the dispersion resulting from the mixing of fine colloidal particles and water

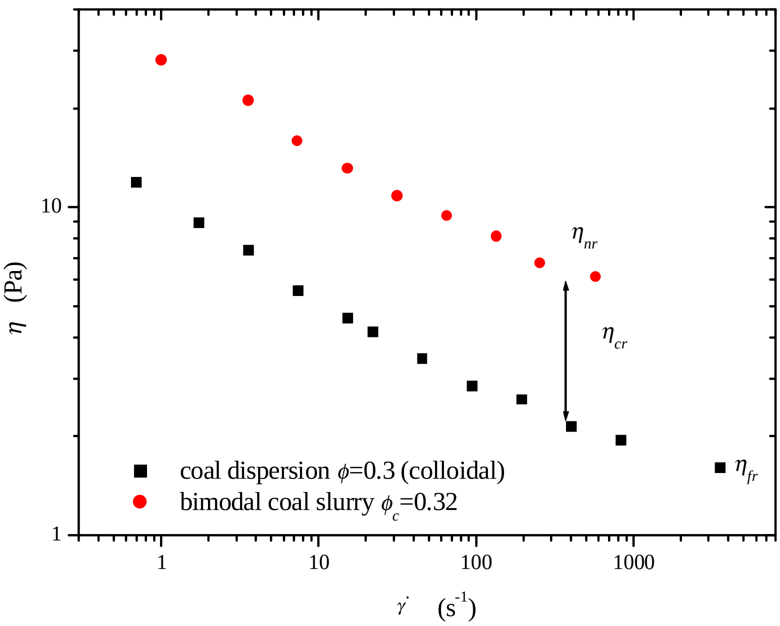

Fig. 9: Variation in the bulk viscosity of coal slurry as a function of the shear rate. The bulk viscosity curve is parallel to the curve obtained with the fine fraction. After (Sengun & Probstein, 1989*a*).

imparts most of its rheological properties to the entire suspension. Secondly, the coarse fraction is assumed to act independently of the fine fraction and to enhance bulk viscosity. They introduced a net viscosity η_{nr} of a bimodal slurry as the product of the fine relative viscosity η_{fr} and the coarse relative viscosity η_{cr}. The fine relative viscosity is defined as the ratio of the apparent viscosity η_f of the fine-particle suspension to the viscosity of the interstitial fluid μ: $\eta_{fr} = \eta_f/\mu$. The coarse relative viscosity is defined as the ratio of the apparent viscosity η_c of the coarse-particle slurry to the viscosity of the fine-particle suspension: $\eta_{cr} = \eta_c/\eta_f$. The two relative viscosities depend on the solid concentrations and a series of generalized Péclet numbers. For the coarse-particle suspensions, all the generalized Péclet numbers are much greater than unity. Using a dimensional analysis, Sengun and Probstein deduced that the coarse relative viscosity cannot depend on shear rate. In contrast, bulk behavior in fine-particle suspensions is governed by colloidal particles and thus at least one of the generalized Péclet numbers is of the order of unity, implying that the fine relative viscosity is shear-dependent. Sengun and Probstein's experiments on the viscosity of coal slurries confirmed the reliability of this concept (Sengun & Probstein, 1989*a*). Plotting $\log \eta_{nr}$ and $\log \eta_{fr}$ against $\log \dot{\gamma}$, they found that over a wide range of concentrations, the curves were parallel and their distance was equal to $\log \eta_{cr}$ (see Fig. 9). However, for solid concentrations in the coarse fraction exceeding 0.35, they observed a significant departure from parallelism which they ascribed to nonuniformity in the shear rate distribution within the bulk due to squeezing effects between coarse particles.

Ancey & Jorrot (2001) examined the effect of adding coarse particles in a colloidal dispersion. At first glance, since the volume occupied by the colloidal particles is decreased, the bulk yield stress should decrease and, to first order, they inferred

$$\tau_c \propto \left(\frac{\phi_f}{1-\phi_f}\right)^c (1-\phi), \tag{7}$$

where ϕ is the coarse-particle concentration and ϕ_f the concentration in fine (colloidal) particles. To test this expectation, Ancey and Jorrot measured the bulk yield stress of kaolin suspensions to which they added a given amount of coarse particles. Figure 10 shows typical results obtained with a bimodal distribution of glass beads (1 mm and 3 mm in diameter). The dimensionless number ξ is the relative fraction of small beads ($\xi = 0$ means that there were no small beads while $\xi = 1$ means that all coarse particles added to the kaolin suspension were small beads). The total solid concentration ϕ_t is computed as follows: $\phi_t = \phi_k(1-\phi_c) + \phi_c$. Comments on Fig. 10 are the following:

- Adding a small amount of coarse particles leads to a decrease in the bulk yield stress (here for total solid concentrations as high as 0.55).
- Interestingly enough, in contrast with the authors' expectation, the bulk yield stress starts diverging when the total solid concentration comes closer to the maximum solid concentration.
- A striking feature of this abrupt rise is that the increase rate is very close to the value measured for a pure kaolin dispersion. This could mean that coarse particles surrounded by colloidal particles may very well behave in turn as colloidal particles (this statement is naturally wrong).
- At low and moderate concentrations of coarse particles, the bulk yield stress was independent of the particle size (when equal size distributions were tested), but it increased significantly with increasing relative fractions of large particles.
- On the contrary, at high concentrations, the finer the distribution, the larger the yield stress.

The main and unexpected result of this experimental study is that bulk yield stress may be significantly affected by the concentration of coarse particles, but its features (such as the growth rate with a solid concentration) are still governed by the fine colloidal fraction.

When the bulk is made up of continuous distribution of particle distributions, the bimodal-suspension approximation is no longer valid. Given substantial experimental difficulties (particle size, sedimentation, etc.), few experimental investigations have been conducted on poorly-sorted slurries. In soil mechanics, testing bulk materials in quasi-static drained or non-drained flow configurations has shown that shear strength is governed by compaction state and pore fluid pressure (Davis & Sevladurai, 2002). Since geotechnical tests can hardly be run under large deformations, Iverson and his colleagues carried out experiments in a 95-m long flume, specifically built in Oregon (USGS flume). In Iverson's opinion, the flow of poorly sorted mixtures is fundamentally an unsteady phenomenon, which cannot be easily investigated under steady flow conditions. Indeed, the shear strength adheres to the Coulomb law: $\tau = \sigma' \tan\varphi$, with $\sigma'{=}\sigma - p$ the

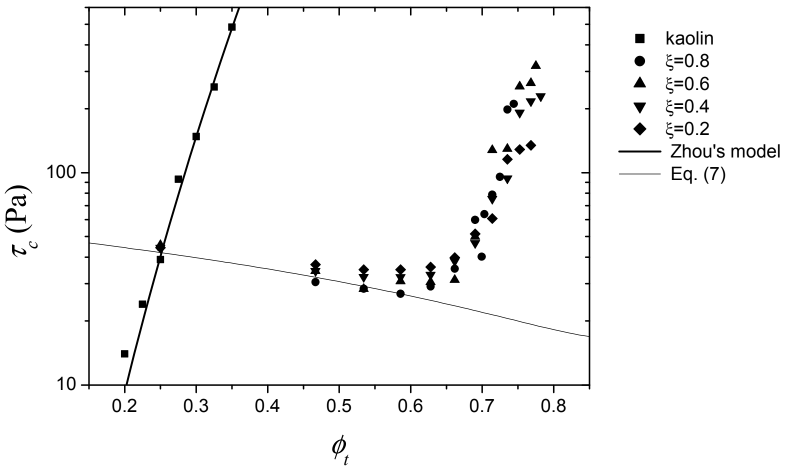

Fig. 10: Variation in the bulk yield stress. The variation in the yield stress for a kaolin suspension is reported as a function of the solid concentration (ϕ_t coincides with the fine fraction). The thin solid line represents the expectation of a decreasing bulk yield stress with increasing coarse concentration [see Eq. (7)]. The symbols represent the experimental data obtained by varying the ratio ξ of large and small beads. The solid thick line stands for the model proposed by Zhou *et al.* (1999) to compute yield stress of concentrated flocculated suspensions. After Ancey & Jorrot (2001).

effective stress. During the motion, the material contracts, which gives rise to high pore pressure and thus a decrease in shear stress. Pore pressure can remain elevated when pore pressure diffusion is slow (i.e., for low bulk permeability). Consequently, shear strength is not a rheological property (Iverson, 2003*a*).

Is it possible to provide clear evidence for the prevalence of Coulomb frictional behavior and dependence of shear strength on pore pressure in rapidly sheared, poorly sorted slurries? Because of the unsteady nature of shear strength together with the number of control variables that are also time-dependent (pore pressure, solid concentration, normal stress), providing an indisputable reply to this question remains difficult. There are, however, a number of laboratory and field observations that support this theory. For instance, carrying out experiments with poorly sorted materials in the USGS flume, Major observed that increasing the fine fraction resulted in thinning the deposit layer, which meant that the bulk strength decreased (Major, 1996) (see also (Iverson, 2003*a*)). This observation conflicts with laboratory experiments showing an increase in yield stress when the fine fraction is increased (see the asymptotic trend in Fig. 10 when $\phi_t \to \phi_m$), but can be explained by recognizing that increasing the fine content leads to a decrease in the bulk permeability and consequently reduces pore pressure diffusion; the bulk stays longer in a liquified state, with high pore-pressure levels and low shear strength. In the next section, we will present laboratory experiments that also provide support for this explanation.

4.3 Application: sheet flows

Here we will examine the consequences of the rheological properties on the flow features for thin free-surface flows (referred to as sheet flows), a typical flow configuration for geophysical flows. In addition to rheological aspects, different flow regimes can occur depending on the relative strength of inertial, pressure, and viscous contributions in the governing equations. Dimensional analysis helps clarify the notions of inertia-dominated and friction-dominated regimes (Ancey & Cochard, 2009; Ancey *et al.*, 2009). We will then focus on creeping flows on gentle slopes and fast flows. In the analytical computations, we will use the shallowness of sheet flows to derive approximate equations. Since the Bingham model is the most studied and widespread constitutive equation, most examples will be based on this model, but we will also refer to papers dealing with alternative viscoplastic models or Coulomb friction.

We consider a shallow layer of fluid flowing over a rigid impermeable plane inclined at an angle θ (see Fig. 11). The fluid is viscoplastic and incompressible; its density is denoted by ρ and its bulk viscosity by $\eta = \tau/\dot{\gamma}$. The ratio $\epsilon = H_*/L_*$ between the typical vertical and horizontal lengthscales, H_* and L_* respectively, is assumed to be small. The streamwise and vertical coordinates are denoted by x and y, respectively.

A two-dimensional flow regime is assumed, namely any cross-stream variation is neglected. The depth of the layer is given by $h(x,\ t)$. The horizontal and vertical velocity components of the velocity $\mathbf{u}$ are denoted by u and v, respectively. The fluid pressure is referred to as $p(x,\ y,\ t)$, where t denotes time. The surrounding fluid (assumed to be air) is assumed to be dynamically passive (i.e., inviscid and low density compared to the moving fluid) and surface tension is neglected, which implies that the stress state at the free surface is zero.

The governing equations are given by the mass and momentum balance

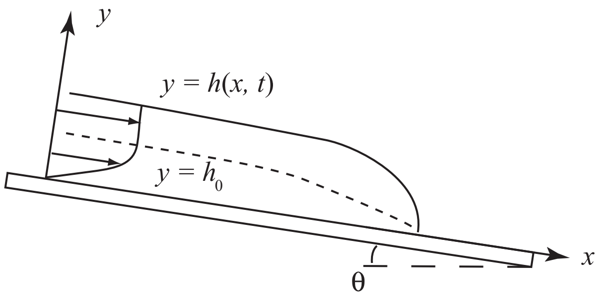

Fig. 11: The configuration of the flow.

equations

$$\nabla \cdot \mathbf{u} = 0, \tag{8}$$

$$\begin{aligned} \rho \frac{\mathrm{d}\mathbf{u}}{\mathrm{d}t} &= \rho \frac{\partial \mathbf{u}}{\partial t} + \rho(\mathbf{u} \cdot \nabla)\mathbf{u} \\ &= \rho \mathbf{g} - \nabla p + \nabla \cdot \boldsymbol{\sigma}, \end{aligned} \tag{9}$$

supplemented by the following boundary conditions at the free surface

$$v(x,h,t) = \frac{\mathrm{d}h}{\mathrm{d}t} = \frac{\partial h}{\partial t} + u(x,h,t)\frac{\partial h}{\partial x}\ , \qquad v(x,0,t) = 0\ . \tag{10}$$

There are many ways of transforming these governing equations into dimensionless expressions (Liu & Mei, 1990*a*; Balmforth & Craster, 1999; Keller, 2003; Ancey & Cochard, 2009). Here we depart slightly from the presentation given by Liu & Mei (1990*a*). The characteristic streamwise and vertical velocities, the timescale, the typical pressure, and the order of magnitude of bulk viscosity are referred to as U_*, V_*, T_*, P_*, and η_*, respectively. Moreover, in addition to the lengthscale ratio ϵ, we introduce the following dimensionless numbers that characterize free-surface, gravity-driven flows: the flow Reynolds number and the Froude number

$$\mathrm{Re} = \frac{\rho U_* H_*}{\eta_*} \text{ and } \mathrm{Fr} = \frac{U_*}{\sqrt{g H_* \cos\theta}}.$$

The following dimensionless variables will be used in this section:

$$\hat{u} = \frac{u}{U_*},\ \hat{v} = \frac{v}{V_*},\ \hat{x} = \frac{x}{L_*},\ \hat{y} = \frac{y}{H_*},\ \text{and } \hat{t} = \frac{t}{T_*}$$

A natural choice for T_* is $T_* = L_*/U_*$. The stresses are scaled as follows:

$$\hat{\sigma}_{xx} = \frac{\eta_* U_*}{L_*}\sigma_{xx},\ \hat{\sigma}_{xy} = \frac{\eta_* U_*}{H_*}\sigma_{xy},\ \hat{\sigma}_{yy} = \frac{\eta_* U_*}{L_*}\sigma_{yy},\ \text{and } \hat{p} = \frac{p}{P_*},$$

where σ_{xx}, σ_{xy}, and σ_{yy} are the normal stress in the x direction, the shear stress, and the normal stress in the x direction, respectively. Here we are interested in free-surface flows. This leads us to set $P_* = \rho g H_* \cos\theta$, since we expect that, to leading order, the pressure adopts a hydrostatic distribution (see below). If we define the vertical velocity scale as $V_* = \epsilon U_*$, the mass balance equation (8) takes the following dimensionless form

$$\frac{\partial \hat{u}}{\partial \hat{x}} + \frac{\partial \hat{v}}{\partial \hat{y}} = 0. \tag{11}$$

Substituting the dimensionless variables into the momentum balance equation (9) leads to

$$\epsilon\mathrm{Re}\frac{\mathrm{d}\hat{u}}{\mathrm{d}\hat{t}} = \frac{\epsilon\mathrm{Re}}{\mathrm{Fr}^2}\left(\frac{1}{\epsilon}\tan\theta - \frac{\partial\hat{p}}{\partial\hat{x}}\right) + \epsilon^2\frac{\partial\hat{\sigma}_{xx}}{\partial\hat{x}} + \frac{\partial\hat{\sigma}_{xy}}{\partial\hat{y}}, \qquad (12)$$

$$\epsilon^3\mathrm{Re}\frac{\mathrm{d}\hat{v}}{\mathrm{d}\hat{t}} = \frac{\epsilon\mathrm{Re}}{\mathrm{Fr}^2}\left(-1 - \frac{\partial\hat{p}}{\partial\hat{y}}\right) + \epsilon^2\frac{\partial\hat{\sigma}_{xy}}{\partial\hat{x}} + \epsilon^2\frac{\partial\hat{\sigma}_{yy}}{\partial\hat{y}}. \qquad (13)$$

The momentum balance equation expresses a balance between gravity acceleration, inertial terms, pressure gradient, and viscous dissipation, whose order of magnitude is $\rho g\sin\theta$, $\rho U_*^2/L_*$, P_*/L_*, and $\eta_* U_*/H_*^2$, respectively. Depending on the values considered for the characteristic scales, different types of flow regime occur. At least four regimes, where two contributions prevail compared to the others, could be achieved in principle

1. *Inertial regime*, where inertial and pressure-gradient terms are of the same magnitude. We obtain
$$U_* = \sqrt{gH_*\cos\theta}.$$
The order of magnitude of the shear stress is $\partial\sigma_{xy}/\partial y = \rho g\, O(\epsilon^{-1}\mathrm{Re}^{-1})$. This regime occurs when: $\epsilon\mathrm{Re} \gg 1$ and $\mathrm{Fr} = O(1)$.

2. *Diffusive regime*, where the pressure gradient is balanced by viscous stresses within the bulk. In that case, we have
$$U_* = \frac{\rho g\cos\theta H_*^3}{\eta_* L_*}.$$
Inertial terms must be low compared to the pressured gradient and the slope must be shallow ($\tan\theta \ll \epsilon$). This imposes the following constraint: $\epsilon\mathrm{Re} \ll 1$. We deduced that $\mathrm{Fr}^2 = O(\epsilon\mathrm{Re}) \ll 1$.

3. *Visco-inertial regime*, where inertial and viscous contributions are nearly equal. In that case, we have
$$U_* = \frac{1}{\epsilon}\frac{\eta_*}{\rho H_*}.$$
The pressure gradient must be low compared to the viscous stress, which entails the following condition $\eta_* \gg \epsilon\rho\sqrt{gH_*^3}$. We obtain $\epsilon\mathrm{Re} \sim 1$ and $\mathrm{Fr} = \eta_*/(\rho\epsilon\sqrt{gH_*^3}) \gg 1$.

4. *Nearly steady uniform regime*, where the viscous contribution matches gravity acceleration. In that case, we have
$$U_* = \frac{\rho g\sin\theta H_*^2}{\eta_*}.$$
Inertia must be negligible, which means $\epsilon \ll 1$ (stretched flows). We obtain $\mathrm{Re} = O(\mathrm{Fr}^2)$ and $\tan\theta \gg \epsilon$ (mild slopes).

In the inertial regime, the rheological effects are so low that they can be neglected and the final governing equations are the Euler equations. The visco-inertial regime is more spurious and has no specific interest in geophysics, notably because the flows are rapidly unstable. More interesting is the diffusive regime that may achieved for very slow flows on gentle slopes ($\theta \ll 1$), typically when flows come to rest, or within the head (Ancey & Cochard, 2009; Ancey *et al.*, 2009). We will further describe this regime in the following. When there is no balance between two contributions, we have to solve the full governing equations. This is usually a difficult task, even numerically. To simplify the problem, one can use flow-depth averaged equations. The nearly-steady regime will be exemplified below within the framework of the kinematic-wave approximation. Finally, it should be kept in mind that the partitioning into four regimes holds for viscous (Newtonian) fluids and non-Newtonian materials for which the bulk viscosity does not vary significantly with shear rate over a sufficiently wide range of shear rates. In the converse case, further dimensionless groups (e.g., the Bingham number $\mathrm{Bi} = \tau_c H_*/(\mu U_*)$) must be introduced, which makes this classification more complicated (Ancey, 2007; Ancey & Cochard, 2009; Ancey *et al.*, 2009).

4.3.1 Slow motion

Slow motion of a viscoplastic material has been investigated by Liu & Mei (1990*a*,*c*), Mei *et al.* (2001), Coussot *et al.* (1996), Balmforth and Craster (Balmforth & Craster, 1999; Balmforth *et al.*, 2002), Matson & Hogg (2007), and Hogg & Matson (2009).

Here we consider that the shear stress is given by (1). Taking the two dominant contributions in Eqs. (12–13) and returning to the physical variables, we deduce

$$\sigma_{xy} = \rho g \cos\theta (h - y) \left(\tan\theta - \frac{\partial h}{\partial x} \right), \tag{14}$$

$$p = \rho g (h - y) \cos\theta. \tag{15}$$

The bottom shear stress is then found to be $\tau_b = \sigma_{xy}|_{y=0}$. For bottom shear stresses in excess of the yield stress τ_c, flow is possible. When this condition is satisfied, there is a yield surface at depth $y = h_0$ within the bulk, along which the shear stress matches the yield stress

$$\sigma_{xy}|_{y=h_0} = \rho g \cos\theta (h - h_0) \left(\tan\theta - \frac{\partial h}{\partial x} \right) = \tau_c. \tag{16}$$

The yield surface separates the flow into two layers (Liu & Mei, 1990*a*; Balmforth & Craster, 1999): the bottom layer, which is sheared, and the upper layer or plug layer, where the shear rate is nearly zero. Indeed, using an asymptotic analysis, (Balmforth & Craster, 1999) demonstrated that in the so-called plug layer, the shear rate is close to zero, but nonzero. This result may seem anecdotic, but it is in fact of great importance since it resolves a number of paradoxes raised about viscoplastic solutions.

On integrating the shear-stress distribution, we can derive a governing equation for the flow depth $h(x,\ t)$. For this purpose, we must specify the constitutive equation. For the sake of simplicity, we consider a Bingham fluid in one-dimensional flows as Liu & Mei (1990*a*) did; the extension to Herschel-Bulkley and/or two-dimensional flows can be found in (Balmforth & Craster, 1999; Balmforth *et al.*, 2002; Mei & Yuhi, 2001; Ancey & Cochard, 2009). In the sheared zone, the velocity profile is parabolic

$$u(y) = \frac{\rho g \cos\theta}{\mu}\left(\tan\theta - \frac{\partial h}{\partial x}\right)\left(h_0 y - \frac{1}{2}y^2\right) \text{ for } y \le h_0,$$

while the velocity is constant to leading order within the plug

$$u(y) = u_0 = \frac{\rho g h_0^2 \cos\theta}{\mu}\left(\tan\theta - \frac{\partial h}{\partial x}\right) \text{ for } y \ge h_0,$$

The flow rate is then

$$q = \int_0^h u(y)\mathrm{d}y = \frac{\rho g h_0^2(3h - h_0)\cos\theta}{6\mu}\left(\tan\theta - \frac{\partial h}{\partial x}\right). \tag{17}$$

Integrating the mass balance equation over the flow depth provides

$$\frac{\partial h}{\partial t} + \frac{\partial q}{\partial x} = 0. \tag{18}$$

Substituting q with its expression (17) and the yield surface elevation h_0 with Eq. (16) into Eq. (18), we obtain a governing equation for h, which takes the form of a nonlinear diffusion equation

$$\frac{\partial h}{\partial t} = \frac{\partial}{\partial x}\left[F(h,\ h_0)\left(\frac{\partial h}{\partial x} - \tan\theta\right)\right], \tag{19}$$

with $F = \rho g h_0^2(3h - h_0)\cos\theta/(6\mu)$.

A typical application of this analysis is the derivation of the shape of a viscoplastic deposit. Contrary to a Newtonian fluid, the flow depth of a viscoplastic fluid cannot decrease indefinitely when the fluid spreads out along an infinite plane. Because of the finite yield stress, when it comes to rest, the fluid exhibits a nonuniform flow-depth profile, where the pressure gradient is exactly balanced by the yield stress. On an infinite horizontal plane, the bottom shear stress must equal the yield stress. Using Eq. (14) with $\theta = 0$ and $y = 0$, we eventually obtain (Liu & Mei, 1990*a*)

$$\sigma_{xy}|_{y=0} = \tau_c = -\rho g h \frac{\partial h}{\partial x}, \tag{20}$$

which, on integrating, provides

$$h(x) - h_i = \sqrt{\frac{2\tau_c}{\rho g}(x_i - x)}, \tag{21}$$

where $h = h_i$ at $x = x_i$ is a boundary condition. This equation shows that the deposit-thickness profile depends on the square root of the distance. This is good agreement with field observations (Coussot *et al.*, 1996); Fig. 12 shows the lobe of debris-flow deposit, whose profile can be closely approximated by (21).

When the slope is nonzero, an implicit solution for $h(x)$ to Eq. (14) is found (Liu & Mei, 1990*a*)

$$\tan\theta(h(x) - h_i) + \frac{\tau_c}{\rho g \cos\theta}\log\left[\frac{\tau_c - \rho g h \sin\theta}{\tau_c - \rho g h_i \sin\theta}\right] = \tan^2\theta(x - x_i). \tag{22}$$

Fig. 12: Lobes of a debris-flow deposit near the Rif Paulin stream (Hautes-Alpes, France).

The shape of a static two-dimensional pile of viscoplastic fluid was investigated by Coussot *et al.* (1996), Mei & Yuhi (2001), Osmond & Griffiths (2001), and Balmforth *et al.* (2002); the latter derived an exact solution, while the former authors used numerical methods or *ad hoc* approximations to solve the two-dimensional equivalent to Eq. (14). Similarity solutions to Eq. (19) have also been provided by Balmforth *et al.* (2002) in the case of a viscoplastic flow down a gently inclined, unconfined surface with a time-varying source at the inlet. Ancey & Cochard (2009) used matched-asymptotic expansions to build approximate analytical solutions for the movement of a finite volume of Herschel-Bulkley fluid down a flume. Matson & Hogg (2007) and Hogg & Matson (2009) investigating the slumping motion of a fixed volume on a plane or down an inclined slope.

4.3.2 Fast motion

The most common method for solving fast-motion free-surface problems is to take the depth-average the local equations of motion. In the literature, this method is referred to as the Saint-Venant approach, the boundary-layer approximation, the lubrication approximation, the long-wave approximation, etc. Here, by fast motion, we refer to situations where inertia, rheological effects, and pressure play a role in flow dynamics. However, flow velocity must not be too high; otherwise instabilities occur at the free surface (Trowbridge, 1987; Liu & Mei, 1990*b*; Balmforth *et al.*, 2004).

The Saint-Venant approach involves integrating the momentum and mass balance equations over the depth. A considerable body of work has been published on this method for Newtonian and non-Newtonian fluids, including viscoplastic (Coussot, 1997; Huang & Garcìa, 1998; Siviglia & Cantelli, 2005) and granular materials (Savage & Hutter, 1989; Gray *et al.*, 1998; Pouliquen & Forterre, 2002; Iverson & Denlinger, 2001; Bouchut *et al.*, 2003; Chugunov *et al.*, 2003; Pudasaini & Hutter, 2003; Kerswell, 2005). Here, we shall briefly recall the principle and then directly provide the resulting governing equations. Let us start with the local mass balance (8). Integrating this equation over the flow depth leads to

$$\int_0^{h(x,t)} \left(\frac{\partial u}{\partial x} + \frac{\partial v}{\partial y}\right) \mathrm{d}y = \frac{\partial}{\partial x} \int_0^h u(x,y,t) \mathrm{d}y - u(h) \frac{\partial h}{\partial x} - v(x,h,t) - v(x,0,t). \tag{23}$$

At the free surface and the bottom, the y-component of velocity v satisfies the boundary conditions (10). We then easily deduce

$$\frac{\partial h}{\partial t} + \frac{\partial h\bar{u}}{\partial x} = 0, \tag{24}$$

where we have introduced depth-averaged variables defined as

$$\bar{f}(x,t) = \frac{1}{h(x,t)} \int_0^{h(x,t)} f(x,y,t) \mathrm{d}y.$$

The same procedure is applied to the momentum balance equation (9). Without any difficulty, we can deduce the averaged momentum equation from the x-component of the momentum equation

$$\bar{\rho} \left(\frac{\partial h\bar{u}}{\partial t} + \frac{\partial h\overline{u^2}}{\partial x}\right) = \bar{\rho} g h \sin\theta - \frac{\partial h\bar{p}}{\partial x} + \frac{\partial h\bar{\sigma}_{xx}}{\partial x} - \tau_b, \tag{25}$$

where we have introduced the bottom shear stress: $\tau_b = \sigma_{xy}(x,0,t)$. In the present form, the system of Eqs. (24–25) is not closed since the number of variables exceeds the number of equations. A common approximation involves introducing a parameter (sometimes called the Boussinesq momentum coefficient), which links the mean velocity to the mean square velocity

$$\overline{u^2} = \frac{1}{h} \int_0^h u^2(y)\, \mathrm{d}y = \alpha \bar{u}^2. \tag{26}$$

Most of the time, the coefficient α is set to unity.

Another helpful (and common) approximation, not mentioned in the above system, concerns the computation of stress. Within the framework of long wave approximation, we assume that longitudinal motion outweighs vertical motion: for any quantity m related to motion, we have $\partial m/\partial y \gg \partial m/\partial x$. This allows us to consider that every vertical slice of flow can be treated as if it was locally uniform. In such conditions, it is possible to infer the bottom shear stress by extrapolating its steady-state value and expressing it as a function of u and h. Using this approximation, Coussot (1994, 1997) obtained the following bottom shear stress

$$\tau_b = \mu \left(\frac{1+2n}{1+n}\right)^n \frac{\bar{u}^n}{h_0^{n+1}((2+n^{-1})h - h_0)^n},$$

for Herschel-Bulkley fluids. Using the first-order approximation of the y-component of the momentum balance equation (9), he found that the pressure was hydrostatic, which leads to a flow-depth averaged pressure

$$\bar{p} = \frac{1}{2}\rho g h \cos\theta.$$

The effects of normal stresses can be neglected to first order. Note that this derivation is not the only way of deriving the Saint-Venant equations for a Bingham fluid; alternative procedures have been proposed (Huang & Garcìa, 1997, 1998; Pastor *et al.*, 2004). For instance, Huang and Garcìa further considered two partial differential equations to supplement the governing equations (24–25) (Huang & Garcìa, 1997, 1998): one equation governing the elevation h_0 of the yield surface and another providing the bottom shear stress.

For Coulomb materials, the same procedure can be repeated. The only modification concerns the momentum balance equation (25), which takes the form (Savage & Hutter, 1989; Iverson & Denlinger, 2001)

$$\bar{\rho}\left(\frac{\partial h\bar{u}}{\partial t} + \frac{\partial h\bar{u}^2}{\partial x}\right) = \bar{\rho} g h \left(\sin\theta - k\cos\theta \frac{\partial h}{\partial x}\right) - \tau_b, \tag{27}$$

with k a proportionality coefficient between the normal stresses $\bar{\sigma}_{xx}$ and $\bar{\sigma}_{yy}$, which is computed by assuming limiting Coulomb equilibrium in compression ($\partial_x \bar{u} < 0$) or extension ($\partial_x \bar{u} > 0$); the coefficient is called the *active/passive pressure* coefficient. In Eq. (27), the bottom shear stress can be computed by using the Coulomb law $\tau_b = (\bar{\sigma}_{yy}|_{y=0} - p_b)\tan\varphi$, with $\bar{\sigma}_{yy}|_{y=0} = \bar{\rho} g h \cos\theta$ and p_b the pore pressure at the bed level.

Analytical solutions can be obtained for the Saint-Venant equations. Most of them were derived by seeking self-similarity solutions; see (Savage & Nohguchi, 1988; Savage & Hutter, 1989; Chugunov *et al.*, 2003) for the Coulomb model and (Hogg & Pritchard, 2004) for viscoplastic and hydraulic models. Some solutions can also be obtained using the method of characteristics. We are going to see two applications based on these methods.

In the first application, we use the fact that the Saint-Venant equations for Coulomb materials are structurally similar to those used in hydraulics when the bottom drag can be neglected. The only difference lies in the nonhydrostatic pressure term and the source term (bottom shear stress). However, using a change in variable makes it possible to retrieve the usual shallow-water equations and seek similarity solutions to derive the Ritter solutions (Mangeney *et al.*, 2000; Karelsky *et al.*, 2000; Kerswell, 2005). The Ritter solutions are the solutions to the so-called dam-break problem, where an infinite volume of material at rest is suddenly released and spreads over a dry bed (i.e., no material laying along the bed). Much attention has been paid to this problem, notably in geophysics because it is used as a paradigm for studying rapid surge motion. We pose

$$x^* = x - \frac{\delta}{2}t^2,\ t^* = t,\ u^* = u - \delta t, \text{ and } h^* = h,$$

where we introduced the parameter $\delta = g\cos\theta(\tan\theta - \mu)$. We deduce

$$\frac{\partial h^*}{\partial t^*} + \frac{\partial h^* u^*}{\partial x^*} = 0, \tag{28}$$

$$\frac{\partial u^*}{\partial t^*}+u^*\frac{\partial u^*}{\partial x^*}+gk\cos\theta\frac{\partial h^*}{\partial x^*}=0. \tag{29}$$

For the dam-break problem, the initial and boundary conditions are

$$\begin{aligned} -\infty<x<\infty,&\ u(x,0)=0,\\ x<0,&\ h(x,0)=h_i,\\ x>0,&\ h(x,0)=0. \end{aligned} \tag{30}$$

The analytical solutions to Eqs. (28–29) are the well-known Ritter solutions. We are looking for a similarity solution in the form (Gratton & Vigo, 1994)

$$\bar{u}^*=t^{*\beta/\alpha}U(\zeta^*) \text{ and } h^*=t^{*\gamma/\alpha}H(\zeta^*),$$

with $\zeta^*=x^*/t^{*\alpha}$ the similarity variable, and H and U two unknown functions. Substituting $\bar{u}^*$ and h^* with their similarity forms into (28–29), we find: $\beta+\alpha=1$ and $\gamma+2\alpha=2$. For this solution to satisfy the initial and boundary conditions, we must pose $\beta=\gamma=0$, hence $\alpha=1$. We then infer

$$\begin{pmatrix} H & U-\zeta^* \\ U-\zeta^* & kg\cos\theta \end{pmatrix}\cdot\begin{pmatrix} U' \\ H' \end{pmatrix}=0,$$

where the prime denotes the ζ^*-derivative. For this system to admit a non-constant solution, its determinant must vanish, which leads to $kgH\cos\theta=(U-\zeta^*)^2$. On substituting this relation into the system above, we deduce $U'=2\zeta^*/3$, thus $U=2(\zeta^*+c)/3$, where c is a constant of integration, $H=4(c-\frac{1}{2}\zeta^*)^2/(9kg\cos\theta)$. The constant c is found using the boundary conditions and by assuming that the undisturbed flow slides at constant velocity δt: $c=\sqrt{kgh_i\cos\theta}$. Returning to the original variables, we find

$$\bar{u}(x,\ t)=\bar{u}^*+\delta t=\frac{2}{3}\left(\frac{x}{t}+\delta t+c\right), \tag{31}$$

$$h(x,\ t)=\frac{1}{9kg\cos\theta}\left(-\frac{x}{t}+\frac{\delta}{2}t+2c\right)^2. \tag{32}$$

The boundary conditions also imply that the solution is valid over the ζ-range $[-c-\delta t,\ 2c+\delta t/2]$; the lower bound corresponds to the upstream condition $\bar{u}=0$, while the upper bound is given by the downstream condition $h=0$. It is worth noting that the front velocity $u_f=2c+\delta t/2$ is constantly increasing or decreasing depending on the sign of δ. When $\delta<0$ (friction in excess of slope angle), the front velocity vanishes at $t=4c/|\delta|$. Figure 13 shows that the shape of the tip region is parabolic at short times ($\delta t\ll c$), in agreement with experimental data (Balmforth & Kerswell, 2005; Siavoshi & Kudrolli, 2005). Solutions corresponding to finite released volumes were also obtained by Ancey *et al.* (2008), Hogg (2006), and Savage & Nohguchi (1988); Savage & Hutter (1989).

In the second application, we use the method of characteristics to find a solution to the governing equations for Bingham flows that are stretched thin when they are nearly steady uniform. For mild slopes, when the aspect ratio ϵ is very low, the inertial and pressure contributions can be neglected (see dimensional analysis above). This means that the flow-depth averaged velocity is very close to the mean velocity reached for steady uniform flows

$$\bar{u}_s=u_p\left(1-\frac{h_0}{3h}\right),$$

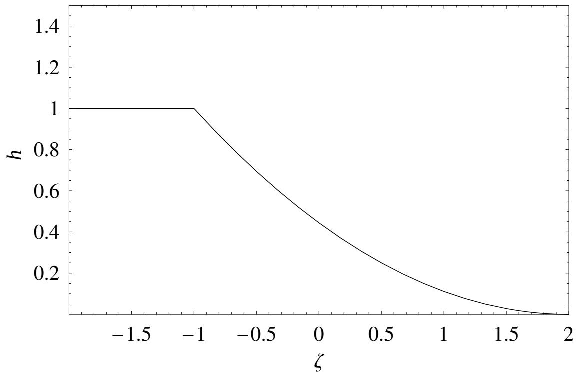

Fig. 13: Flow-depth profile generated just after the wall retaining a granular material is removed. Computations made with $c = 1$ m/s. The similarity variable ζ is $\zeta = x/t$.

where u_p is the plug velocity

$$u_p = \frac{\rho g h_0^2 \sin\theta}{2\mu},$$

with h the flow depth and $h_0 = h - \tau_c/(\rho g \sin\theta)$ the yield-surface elevation; h_0 must be positive or no steady flow occurs. We then use the kinematic-wave approximation introduced by Lighthill & Whitham (1955) to study floods on long rivers; this approximation was then extensively used in hydraulic applications (Weir, 1983; Arattano & Savage, 1994; Hunt, 1994; Huang & Garcìa, 1997, 1998). It involves substituting the mean velocity into the mass balance equation (24) by its steady-state value

$$\frac{\partial h}{\partial t} + \frac{\partial}{\partial x} u_p \left(h - \frac{h_0}{3} \right) = 0. \tag{33}$$

Introducing the plug thickness $h_p = h - h_0 = \tau_c/(\rho g \sin\theta)$, we obtain an expression that is a function of h and its time and space derivative

$$\frac{\partial h}{\partial t} + K\left(h^2 - h h_p\right)\frac{\partial h}{\partial x} = 0,$$

with $K = \rho g \sin\theta/\mu$. The governing equation takes the form of a nonlinear advection equation, which can be solved using the method of characteristics (LeVeque, 2002).

Using the chain rule for interpreting this partial differential equation (33), we can show that it is equivalent to the following ordinary equation

$$\frac{\mathrm{d}h}{\mathrm{d}t} = 0, \tag{34}$$

along the characteristic curve

$$\frac{\mathrm{d}x}{\mathrm{d}t} = \lambda(h), \tag{35}$$

in the $(x,\ t)$ plane, with $\lambda(h) = Kh\,(h - h_p)$. Equation (34) shows that the flow depth is constant along the characteristic curve, hence the characteristic curves are straight lines, the slope of which are given by the right-hand side term $\lambda(h)$ in Eq. (35). These characteristic curves can be used to solve an initial value problem, where the initial value of h is known over a given interval: $h = h_i(x_i)$ (at $t = 0$). The value of h along each characteristic curve is the value of h at the initial point $x(0) = x_i$. We can thus write

$$h(x,\ t) = h_i(x_i) = h_i(x - \lambda(h_i(x_i))t).$$

It is worth noting that because of the nonlinearity of Eq. (33), a smooth initial condition can generate a discontinuous solution (shock) if the characteristic curves intersect, since at the point of intersection h takes (at least) two values (LeVeque, 2002).

References

Ancey, C. 2001 Role of lubricated contacts in concentrated polydisperse suspensions. *J. Rheol.* **45**, 1421–1439.

Ancey, C. 2007 Plasticity and geophysical flows: A review. *J. Non-Newtonian Fluid Mech.* **142**, 4–35.

Ancey, C. & Cochard, S. 2009 The dam-break problem for Herschel-Bulkley fluids down steep flumes. *J. Non-Newtonian Fluid Mech.* **158**, 18–35.

Ancey, C., Cochard, S. & Andreini, N. 2009 The dam-break problem for viscous fluids in the high-capillary-number limit. *J. Fluid Mech.* **624**, 1–22.

Ancey, C. & Coussot, P. 1999 Transition from frictional to viscous regime for granular suspensions. *C. R. Acad. Sci. Paris sér. I* **327**, 515–522.

Ancey, C. & Evesque, P. 2000 Frictional-collisional regime for granular suspension flows down an inclined channel. *Phys. Rev. E* **62**, 8349–8360.

Ancey, C., Iverson, R.M., Rentschler, M. & Denlinger, R. P. 2008 An exact solution for ideal dam-break floods on steep slopes. *Water Resour. Res.* **44**, W01430.

Ancey, C. & Jorrot, H. 2001 Yield stress for particle suspensions within a clay dispersion. *J. Rheol.* **45**, 297–319.

Aragon, J.A. 1995 Granular-fluid chute flow: experimental and numerical observations. *J. Hydraul. Eng.* **121**, 355–364.

Arattano, M. & Savage, W.Z. 1994 Modelling of debris flows as kinematic waves. *Bull. Int. Assoc. Eng. Geol.* **49**, 3–13.

Armanini, A., Capart, H., Fraccarollo, L. & Larcher, M. 2005 Rheological stratification in experimental free-surface flows of granular-liquid mixtures. *J. Fluid Mech.* **532**, 269–319.

Armanini, A. & Gregoretti, C. 2005 Incipient sediment motion at high slopes in uniform flow condition. *Water Resour. Res.* **41**, W12431.

Balmforth, N.J. & Craster, R.V. 1999 A consistent thin-layer theory for Bingham plastics. *J. Non-Newtonian Fluid Mech.* **84**, 65–81.

Balmforth, N.J., Craster, R.V. & Sassi, R. 2002 Shallow viscoplastic flow on an inclined plane. *J. Fluid Mech.* **470**, 1–29.

Balmforth, N.J., Craster, R.V. & Sassi, R. 2004 Dynamics of cooling viscoplastic domes. *J. Fluid Mech.* **499**, 149–182.

Balmforth, N.J. & Kerswell, R.R. 2005 Granular collapse in two dimensions. *J. Fluid Mech.* **538**, 399–428.

Bardou, E., Ancey, C., Bonnard, C. & Vulliet, L. 2003 Classification of debris-flow deposits for hazard assessment in alpine areas. In *Debris Flow Mechanics and Mitigation Conference* (ed. C.L. Chen & D. Rickenmann), pp. 799–808. Davos: Mills Press.

Bardou, E., Bardou, Bowen, P., Boivin, P. & Banfill, P. 2007 Impact of small amounts of swelling clays on the physical properties of debris-flow-like granular materials. Implication for the study of alpine debris flow. *Earth Surf. Processes Landforms* **32**, 698–710.

Bernard, C.J.M. 1927 *Cours de restauration des montagnes*. Nancy: École Nationale des Eaux et Forêts.

Bird, R.B., Dai, G.C. & Yarusso, B.J. 1983 The rheology and flow of viscoplastic materials. *Rev. Chem. Eng.* **1**, 1–70.

Bouchut, F., Mangeney-Castelnau, A., Perthame, B. & Vilotte, J.-P. 2003 A new model of Saint Venant and Savage-Hutter type for gravity driven shallow flows. *C. R. Acad. Sci. Paris sér. I* **336**, 531–536.

Brunsden, D. & Prior, D.B., ed. 1984 *Slope Instability*. New York: John Wiley & Sons.

Chambon, G., Ghemmour, A. & Laigle, D. 2009 Gravity-driven surges of a viscoplastic fluid: an experimental study. *J. Non-Newtonian Fluid Mech.* **158**, 54–62.

Chen, C.-L. 1987 Comprehensive review of debris flow modeling concepts in Japan. *Rev. Eng. Geol.* **7**, 13–29.

Chugunov, V., Gray, J.M.N.T. & Hutter, K. 2003 Group theoretic methods and similarity solutions of the Savage-Hutter equations. In *Dynamics Response of Granular and Porous Materials under Large and Catastrophic Deformations* (ed. K. Hutter & N. Kirchener), pp. 251–261. Berlin: Springer.

Church, M. 2006 Bed material transport and the morphology of alluvial river channels. *Annual Review of Earth and Planetary Sciences* **34**, 325–354.

Coe, J.A., Kinner, D.A. & Godt, J.W. 2008 Initiation conditions for debris flows generated by runoff at Chalk cliffs, central Colorado. *Geomorphology* **96**, 270–297.

Contreras, S.M. & Davies, T.R.H. 2000 Coarse-grained debris-flows: hysteresis and time-dependent rheology. *J. Hydraul. Eng.* **126**, 938–941.

Coussot, P. 1994 Steady, laminar, flow of concentrated mud dispensions in open channel. *J. Hydraul. Res.* **32**, 535–559.

Coussot, P. 1997 *Mudflow Rheology and Dynamics*. Rotterdam: Balkema.

Coussot, P., Laigle, D., Arratano, M., Deganutti, A. & Marchi, L. 1998 Direct determination of rheological characteristics of debris flow. *J. Hydraul. Eng.* **124**, 865–868.

Coussot, P. & Meunier, M. 1996 Recognition, classification and mechanical description of debris flows. *Earth Science Review* **3-4**, 209–227.

Coussot, P., Nguyen, Q.D., Huynh, H.T. & Bonn, D. 2002 Viscosity bifurcation in thixotropic, yielding fluids. *J. Rheol.* **46**, 573–590.

Coussot, P. & Piau, J.M. 1995 A large-scale field coaxial cylinder rheometer for the study of the rheology of natural coarse suspensions. *J. Rheol.* **39**, 105–124.

Coussot, P., Proust, S. & Ancey, C. 1996 Rheological interpretation of deposits of yield stress fluids. *J. Non-Newtonian Fluid Mech.* **66**, 55–70.

Coussot, P., Raynaud, J.S. & Ancey, C. 2003 Combined MRI-rheometry determination of the behavior of mud suspensions. In *Debris Flow Mechanics and Mitigation Conference* (ed. C.-L. Chen & D. Rickenmann), pp. 291–301. Davos: Mills Press.

Davies, T.R.H. 1986 Large debris flow: a macro-viscous phenomenon. *Acta Mech.* **63**, 161–178.

Davis, R.O. & Sevladurai, A.P.S. 2002 *Plasticity and Geomechanics*. Cambridge: Cambridge University Press.

Denlinger, R.P. & Iverson, R.M. 2001 Flow of variably fluidized granular masses across three-dimensional terrain. 2. Numerical predictions and experimental tests. *J. Geophys. Res.* **106**, 553–566.

Egashira, S., Itoh, T. & Takeushi, H. 2001 Transition mechanics of debris flows over rigid bed to over erodible bed. *Phys. Chem. Earth B* **26**, 169–174.

Félix, G. & Thomas, N. 2004 Relation between dry granular flow regimes and morphology of deposits: formation of levées in pyroclastic deposits. *Earth Planet. Sci. Lett.* **221**, 197–213.

Garcia, C., Cohen, H., Reid, I., Rovira, A., Úbeda, X. & Laronne, J.B. 2007 Processes of initiation of motion leading to bedload transport in gravel-bed rivers. *Geophys. Res. Lett.* **34**, L06403.

Gratton, J. & Vigo, C. 1994 Self-similar gravity currents with variable inflow revisited: plane currents. *J. Fluid Mech.* **258**, 77–104.

Gray, J.M.N.T., Wieland, M. & Hutter, K. 1998 Gravity-driven free surface flow of granular avalanches over complex basal topography. *Proc. R. Soc. London ser. A* **455**, 1841–1874.

Hogg, A.J. 2006 Lock-release gravity currents and dam-break flows. *J. Fluid Mech.* **569**, 61–87.

Hogg, A.J. & Matson, G.P. 2009 Slumps of viscoplastic fluids on slopes. *J. Non-Newtonian Fluid Mech.* **158**, 101–112.

Hogg, A.J. & Pritchard, D. 2004 The effects of hydraulic resistance on dam-break and other shallow inertial flows. *J. Fluid Mech.* **501**, 179–212.

Huang, X. & Garcìa, M.H. 1997 A perturbation solution for Bingham-plastic mudflows. *Journal of Hydraulic Engineering* **123**, 986–994.

Huang, X. & Garcìa, M.H. 1998 A Herschel-Bulkley model for mud flow down a slope. *J. Fluid Mech.* **374**, 305–333.

Hunt, B. 1994 Newtonian fluid mechanics treatment of debris flows and avalanches. *J. Hydraul. Eng.* **120**, 1350–1363.

Iverson, R.M. 1997 The physics of debris flows. *Rev. Geophys.* **35**, 245–296.

Iverson, R.M. 2003*a* The debris-flow rheology myth. In *Debris flow Mechanics and Mitigation Conference* (ed. C.L. Chen & D. Rickenmann), pp. 303–314. Davos: Mills Press.

Iverson, R.M. 2003*b* How should mathematical models of geomorphic processus be judged? In *Prediction in Geomorphology* (ed. P.R. Wilcock & R.M. Iverson), pp. 83–94. Washington, D.C.: American Geophysical Union.

Iverson, R.M. 2005 Debris-flow mechanics. In *Debris-flow hazards and related phenomena* (ed. M. Jakob & O. Hungr), pp. 105–134. Berlin: Springer.

Iverson, R.M. & Denlinger, R.P. 2001 Flow of variably fluidized granular masses across three-dimensional terrain. 1. Coulomb mixture theory. *J. Geophys. Res.* **106**, 537–552.

Iverson, R.M., Reid, M.E. & LaHusen, R.G. 1997 Debris-flow mobilization from landslides. *Annual Review of Earth and Planetary Sciences* **25**, 85–138.

Jenkins, J.T. 1994 Rapid granular flow down inclines. *Appl. Mech. Rev.* **47**, 240–244.

Johnson, A.M. & Rodine, J.R. 1984 Debris flow. In *Slope Instability* (ed. D. Brunsden & D.B. Prior), pp. 257–362. Chichester: John Wiley & Sons.

Jop, P., Forterre, Y. & Pouliquen, O. 2005 Crucial role of side walls for granular surface flows: consequences for the rheology. *J. Fluid Mech.* **541**, 167–192.

Josserand, C., Lagrée, P.-Y. & Lhuillier, D. 2004 Stationary shear flows of dense granular materials: a tentative continuum modelling. *Eur. Phys. J. E* **14**, 127–135.

Karelsky, K.V., Papkov, V.V., Petrosyan, A.S. & Tsygankov, D.V. 2000 Particular solutions of shallow-water equations over a non-flat surface. *Phys. Lett. A* **271**, 341–348.

Keller, J.B. 2003 Shallow-water theory for arbitrary slopes of the bottom. *J. Fluid Mech.* **489**, 345–348.

Kerswell, R.R. 2005 Dam break with Coulomb friction: a model for granular slumping? *Phys. Fluids* **17**, 057101.

LeVeque, R.J. 2002 *Finite Volume Methods for Hyperbolic Problems*. Cambridge: Cambridge University Press.

Lighthill, M.J. & Whitham, G.B. 1955 On kinematic waves. I. Flood movement in long rivers. *Proc. R. Soc. London ser. A* **229**, 281–316.

Liu, K.F. & Mei, C.C. 1990*a* Approximate equations for the slow spreading of a thin sheet of Bingham plastic fluid. *Phys. Fluids* **A 2**, 30–36.

Liu, K.F. & Mei, C.C. 1990*b* Roll waves on a layer of a muddy fluid flowing down a gentle slope – A Bingham model. *Phys. Fluids* **6**, 2577–2590.

Liu, K.F. & Mei, C.C. 1990*c* Slow spreading of a sheet of Bingham fluid on an inclined plane. *J. Fluid Mech.* **207**, 505–529.

Lootens, D., Van Damme, H. & Hébraud, P. 2003 Giant stress fluctuations at the jamming transition. *Phys. Rev. Lett.* **90**, 178301.

Major, J.J. 1996 Experimental Studies of Deposition of Debris Flows: Process, Characteristics of Deposits, and Effects of Pore-Fluid Pressure. Ph.d., Washington.

Major, J.J. 1997 Depositional processes in large-scale debris-flow experiments. *J. Geol.* **105**, 345–366.

Major, J.J. 2000 Gravity-driven consolidation of granular slurries – Implications for debris-flow deposition and deposit characteristics. *J. Sediment. Res.* **70**, 64–83.

Major, J.J., Iverson, R.M., McTigue, D.F., Macias, S. & Fiedorowicz, B.K. 1997 Geotechnical properties of debris-flow sediments and slurries. In *Debris Flow Mechanics and Mitigation Conference* (ed. C.-L. Chen), pp. 249–259.

Major, J.J. & Pierson, T.C. 1992 Debris flow rheology: experimental analysis of fine-grained slurries. *Water Resour. Res.* **28**, 841–857.

Mangeney, A., Heinrich, P. & Roche, R. 2000 Analytical solution for testing debris avalanche numerical models. *Pure Appl. Geophys.* **157**, 1081–1096.

Marquez, M., Robben, A., Grady, B.P. & Robb, I. 2006 Viscosity and yield stress reduction in non-colloidal concentrated suspensions by surface modification with polymers and surfactants and/or nanoparticle addition. *J. Colloid. Interface Sci.* **295**, 374–387.

Martino, R. 2003 Experimental analysis on the rheological properties of a debris-flow deposit. In *Debris Flow Mechanics and Mitigation Conference* (ed. C.L. Chen & D. Rickenmann), pp. 363–373. Davos: Mills Press.

Matson, G.P. & Hogg, A.J. 2007 Two-dimensional dam break flows of Herschel-Bulkley fluids: the approach to the arrested state. *J. Non-Newtonian Fluid Mech.* **142**, 79–94.

Mei, C.C., Liu, K.F. & Yuhi, M. 2001 Mud flows – Slow and fast. In *Geomorphological Fluid Mechanics: selected topics in geological and geomorphological fluid mechanics* (ed. N.J. Balmforth & A. Provenzale), pp. 548–577. Berlin: Springer.

Mei, C.C. & Yuhi, M. 2001 Slow flow of a Bingham fluid in a shallow channel of finite width. *J. Fluid Mech.* **431**, 135–159.

Montgomery, D.R. & Buffington, J.M. 1997 Channel-reach morphology in mountain drainage basins. *Geol. Soc. Amer. Bull.* **109**, 596611.

Montgomery, D.R., Schmidt, K.M., Dietrich, W.E. & McKean, J. 2009 Instrumental record of debris flow initiation during rainfall: implications for modeling slope stability. *J. Geophys. Res.* **114**, F01031.

Nishimura, K., Keller, S., McElwaine, J. & Nohguchi, Y. 1998 Ping-pong ball avalanche at a ski jump. *Granul. Matter* **1**, 51–56.

O'Brien, J.S. & Julien, P.Y. 1988 Laboratory analysis of mudflow properties. *J. Hydraul. Eng.* **114**, 877–887.

Osmond, D.I. & Griffiths, R.W. 2001 The static shape of yield strength fluids slowly emplaced on slopes. *J. Geophys. Res.* **B 106**, 16241–16250.

Papanastasiou, T.C. 1987 Flows of materials with yield. *J. Rheol.* **31**, 385–404.

Parsons, J.D., Whipple, K.X. & Simoni, A. 2001 Experimental study of the grain-flow, fluid-mud transition in debris flows. *J. Geol.* **109**, 427–447.

Pastor, M., Quecedo, M., González, E., Herreros, M.I., Fernández, J.A. & Mira, P. 2004 Simple approximation to bottom friction for Bingham fluid depth integrated models. *J. Hydraul. Eng.* **130**, 149–155.

Phillips, C.J. & Davies, T.R.H. 1991 Determining rheological parameters of debris flow material. *Geomorphology* **4**, 101–110.

Pouliquen, O. & Forterre, Y. 2002 Friction law for dense granular flow: application to the motion of a mass down a rough inclined plane. *J. Fluid Mech.* **453**, 133–151.

Pudasaini, S.P. & Hutter, K. 2003 Rapid shear flows of dry granular masses down curved and twisted channels. *J. Fluid Mech.* **495**, 193–208.

Remaître, A., Malet, J.-P., Maquaire, O., Ancey, C. & Locat, J. 2005 Flow behaviour and runout modelling of a complex debris flow in a clay-shale basin. *Earth Surf. Processes Landforms* pp. 479–488.

RICKENMANN, D. 1992 Hyperconcentrated flow and sediment transport at steep slopes. *J. Hydraul. Eng.* **117**, 1419–1439.

RICKENMANN, D. 1997 Sediment transport in Swiss torrents. *Earth Surf. Processes Landforms* **22**, 937–951.

RICKENMANN, D. 1999 Empirical relationships for debris flows. *Nat. Hazard* **19**, 47–77.

RICKENMANN, D. & ZIMMERMANN, M. 1993 The 1987 debris flows in Switzerland: documentation and analysis. *Geomorphology* **8**, 175–189.

SAVAGE, S.B. 1982 Granular flows down rough inclined - Review and extension. In *U.S./ Japan Seminar on New Models and Constitutive Relations in the Mechanics of Granular Materials* (ed. J.T. Jenkins & M. Satake), pp. 261–282. Ithaca: Elseviers Science Publishers, Amsterdam.

SAVAGE, S.B. & HUTTER, K. 1989 The motion of a finite mass of granular material down a rough incline. *J. Fluid Mech.* **199**, 177–215.

SAVAGE, S.B. & NOHGUCHI, Y. 1988 Similarity solutions for avalanches of granular materials down curved bed. *Acta Mech.* **75**, 153–174.

SCHATZMANN, M., FISCHER, P.F. & BEZZOLA, G.R. 2003 Rheological behavior of fine and large particle suspensions. *J. Hydraul. Eng.* **129**, 796–803.

SCOTT, K.M. 1988 Origins, behavior, and sedimentology of lahars and lahars-runout flows in the Toutle-Cowlitz river system. *Tech. Rep.*. U.S. Geological Survey Professional paper 1447-A.

SENGUN, M.Z. & PROBSTEIN, R.F. 1989*a* Bimodal model of slurry viscosity with applications to coal slurries. Part 1. Theory and experiment. *Rheol. Acta* **28**, 382–393.

SENGUN, M.Z. & PROBSTEIN, R.F. 1989*b* Bimodal model of slurry viscosity with applications to coal slurries. Part 2. High shear limit behaviour. *Rheol. Acta* **28**, 394–401.

SIAVOSHI, S. & KUDROLLI, A. 2005 Failure of a granular step. *Phys. Rev. E* **71**, 051302.

SIVIGLIA, A. & CANTELLI, A. 2005 Effect of bottom curvature on mudflow dynamics: Theory and experiments. *Water Resour. Res.* **41**, W11423.

SMART, G.M. & JAEGGI, M.N.R. 1983 Sedimenttransport in steilen Gerinnen. *Tech. Rep.* 64. Mitteilungen n 64 der Versuchanstalt für wasserbau, Hydrologie und Glaziologie.

SOSIO, R. & CROSTA, G.B. 2009 Rheology of concentrated granular suspensions and possible implications for debris flow modeling. *Water Resour. Res.* **45**, W03412.

TAKAHASHI, T. 1981 Debris flow. *Annu. Rev. Fluid Mech.* **13**, 57–77.

TAKAHASHI, T. 1991 *Debris flow*. Rotterdam: Balkema.

TOGNACCA, C. 1999 Beitrag zur Untersuchung der Entstehungsmechanismen von Murgängen. PhD thesis, Eidgenössischen Technischen Hochschule Zürich.

TROWBRIDGE, J.H. 1987 Instability of concentrated free surface flows. *J. Geophys. Res.* **C 92**, 9523–9530.

TSAI, J.-C., LOSERT, W. & VOTH, G.A. 2001 Two-dimensional granular Poiseuille flow on an incline: Multiple dynamical regimes. *Phys. Rev. E* **65**, 011306.

TUBINO, M. & LANZONI, S. 1993 Rheology of debris flows: experimental observations and modelling problems. *Excerpta* **7**, 201–235.

VOIGHT, B. 1990 The 1985 Nevado del Ruiz volcano catastrophe: anatomy and restropection. *J. Volcan. Geoth. Res.* **44**, 349–386.

WAN, Z. & WANG, Z. 1994 *Hypercontrated flow*. Rotterdam: Balkema.

WEIR, G.J. 1983 The asymptotic behaviour of simple kinematic waves of finite volume. *Proc. R. Soc. London ser. A* **387**, 459–467.

WILSON, S.K., DUFFY, B.R. & ROSS, A.B. 2002 On the gravity-driven draining of a rivulet of a viscoplastic material down a slowly varying substrate. *Phys. Fluids* **14**, 555–571.

WOHL, E. 2000 *Mountain Rivers*. Washington: American Geophysical Union.

ZHOU, Z., SOLOMON, M.J., SCALES, P.J. & BOGER, D.V. 1999 The yield stress of concentrated flocculated suspensions of size distributed particles. *J. Rheol.* **43**, 651–671.

ZHU, H., KIM, Y.D. & DE KEE, D. 2005 Non-Newtonian fluids with a yield stress. *J. Non-Newtonian Fluid Mech.* **129**, 177–181.

ZIMMERMANN, M., MANI, P., GAMMA, P., GSTEIGER, P., HEINIGER, O. & HUNIZKER, G. 1997 *Murganggefahr und Klimaänderung - ein GIS-basierter Ansatz*. Zürich: VDF.